

Unified Dynamic Approach for Simulating Quantum Tunneling and Thermionic Emission at Metal-Organic Interfaces

Jiaqing Huang¹, Yijie Mo¹, and Yao Yao^{1*}*Department of Physics and State Key Laboratory of Luminescent Materials and Devices, South China University of Technology, Guangzhou 510640, China* (Received 27 October 2020; revised 4 December 2020; accepted 9 December 2020; published 13 January 2021)

Injection from metallic electrodes serves as a main channel of charge generation in organic semiconducting devices and the quantum effect is normally regarded as essential. We develop a dynamic approach based upon the surface-hopping (SH) algorithm and classical device modeling, by which both quantum tunneling and thermionic emission of charge-carrier injection at metal-organic interfaces are concurrently investigated. The injected charges from a metallic electrode are observed to spread quickly onto the organic molecules, followed by an accumulation close to the interface, induced by the built-in electric field. We compare the Ehrenfest dynamics on the mean-field level and the SH algorithm by simulating the temperature dependence of the charge-injection dynamics and it is found that the former leads to an improper result, that the injection efficiency decreases with increasing temperature in the room-temperature regime while the SH results are credible. The relationship between the injected charges and the applied bias voltage suggests that it is the quantum tunneling that dominates the low-threshold injection characteristics in molecular crystals, which is further supported by the calculation results of a small entropy change during the injection process. An optimum interfacial width for the charge-injection efficiency at the interface is also quantified and can be utilized to understand the role of the interfacial buffer layer in practical devices.

DOI: [10.1103/PhysRevApplied.15.014021](https://doi.org/10.1103/PhysRevApplied.15.014021)

I. INTRODUCTION

The successful industrial application of organic light-emitting devices (OLEDs) might be one of the great scientific achievements of recent decades. Researchers are still devoting efforts to improving the efficiency so that OLEDs can be extended to more application scenarios, such as illumination, and more comprehensive analysis of the microscopic working mechanism is thus highly in demand [1–9]. So far, several ingredients such as the molecular structure [1,2], the interfacial dipole [3–5], and the contact resistance [6–9] have served as the key issues for improving device performance. In particular, due to cost control, the organic semiconductors are normally in the amorphous phase and the contacts between the conducting layer and electrodes are regarded as poor. Moreover, unlike the inorganic semiconductors, in which intentional doping gives rise to numerous charge carriers, the main source of carriers in organic semiconductors stems from metallic electrodes. Therefore, the injection efficiency at the metal-organic interface has a significant impact on the overall performance of organic semiconducting devices.

In statistical physics, the charge injection at interfaces can be described well by the Richardson formula in the

framework of thermionic emission theory [10]. This theory is valid when the concentration of doped charges in inorganic semiconductors is sufficiently large that the injected carriers will not drive the system far away from thermal equilibrium and the detailed balance principle is relevant. In this perspective, given the structure of the single-electron energy spectrum, it is possible to derive the injected current and the details of the dynamical processes are not important. On the experimental side, therefore, techniques such as ultraviolet photoelectron spectroscopy are widely used to study the energy-level alignment at these interfaces and thus the magnitude of the barrier for charge injection can be determined [11–14]. In contrast to the inorganic semiconductors, charge injection at metal-organic interfaces dominates the generation and interfacial recombination of charge carriers. Either thermionic emission or quantum tunneling may play the key role in charge injection. Since the semiconductors are almost without free charges in the initial (as-prepared) stage, the injected charge easily forces the system into the nonequilibrium state and the dynamical process of injection turns out to be essential. In addition, organic materials normally possess strong electron-phonon interactions, making the intrinsic mechanisms of charge injection more complicated [15].

In recent years, mixed quantum-classical dynamics (MQCD) have become an important tool with which to study charge injection and transport properties in organic

*yaoyao2016@scut.edu.cn

semiconductors [16–26]. The MQCD can be generally performed in two different ways: via the Ehrenfest dynamics or the surface-hopping (SH) algorithm. The Ehrenfest dynamics based on the mean-field theory have a simple formulation in which the mean trajectory evolves on an effective potential-energy surface (PES) for the electronic states and it has been applied to charge injection in organic semiconductors by several groups [27–31]. By simulating the electron injection in a metal-polymer-metal structure, Wu and co-workers have found that the injection of electrons finally leads to the formation of polarons or bipolarons and that the electric field applied on the polymer can effectively reduce the interfacial potential barrier for charge injection from the metallic electrode to the polymer [27,28]. Similarly, Johansson and Stafström have simulated the formation of polarons in an isolated polymer chain [29], while Fu and co-workers have considered a similar issue in a metal-polymer structure [30]. More recently, Ribeiro Junior and da Cunha have obtained polaron-type products through careful investigations of the hole-injection dynamics in polymers [31]. In these works, the Ehrenfest dynamics are performed in the framework of the tight-binding Su-Schrieffer-Heeger model to describe the dynamic properties of the charge-injection process. Although this works well for the simulation of elementary quasiparticles, the method merely takes one effective PES into account and is not satisfactory when there is a large barrier and the quantum tunneling is remarkable. The discussion of charge injection in practical organic semiconductors is still one of the prominent topics, especially when device physicists want to understand the role of realistic device parameters such as the electric field, the interfacial morphology, and so on.

It is known that due to the strong interaction between electrons and phonons, organic systems may undergo nonadiabatic transitions among different PESs. The nonadiabatic phenomena are very common in a large number of situations, such as atomic and molecular collision reactions, molecular photochemistry and photophysics, and photoexcitation of condensed-phase systems [21,22]. In recent years, the SH algorithm has become a crucial tool for the dynamic propagation of nonadiabatic systems in physics, chemistry, and the material sciences [21–26]. In this algorithm, the nuclei move on an active PES with respect to the classical Newton equation and perform stochastic hops among different PESs based on the population flux among adiabatic electronic states. Tully’s standard fewest-switches surface hopping and the related algorithms that were developed have been used successfully to study the charge transport in molecular crystals: the results always highlight the importance of nonadiabatic transitions or quantum tunneling for organic semiconductors [32–39]. The present work is thus motivated to provide a unified approach based on the SH algorithm to simulate the charge-injection process for different situations,

regardless of whether quantum tunneling or thermionic emission is predominant.

As a typical organic semiconducting material, rubrene possesses large mobility and has attracted much research interest recently due to its low-threshold injection characteristics in heterojunction devices [40–44]. In this work, by embedding the classical Poisson’s equation into the standard SH algorithm, the nonadiabatic dynamics of charge injection at metal-organic interfaces are investigated within the framework of a molecular-crystal model. The generation of the injected charges is discussed first. The injected charges calculated by the SH algorithm are then compared with the results from the Ehrenfest dynamics. The influence of the bias voltage applied at the metallic electrode on the injected charges and the optimum width of the interfacial layer for charge injection are investigated. Finally, the charge-injection process at the metal-organic interface is detailed in terms of the evolution of the entropy change. The paper is organized as follows. The model for the metal-organic system and the dynamic evolution method are given in Sec. II. The results and discussion are presented in Sec. III. Finally, in Sec. IV, the main conclusions are drawn.

II. MODEL AND METHOD

Throughout this work, we use rubrene as an example to show the simulation results from our developed dynamic

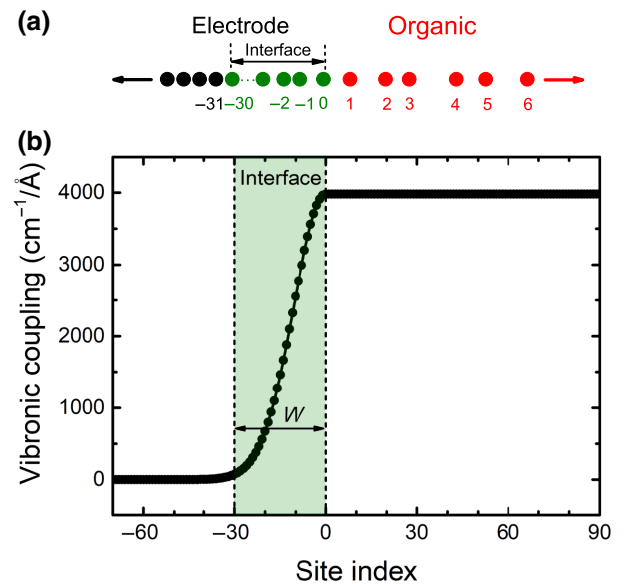


FIG. 1. (a) A schematic diagram of the structure of our model. The black dots on the left represent the atoms of the metallic electrode, which do not move, and the red dots on the right are organic molecules with random thermal motions, respectively. Thirty green dots in the middle part denote the interface. (b) The distribution of the vibronic coupling strength at each site, where W is the width of the interfacial layer.

approach. Without loss of generality, a metallic electrode and the rubrene molecules are placed head to tail to construct a one-dimensional metal-organic heterojunction, as sketched in Fig. 1(a), in which 160 sites in total are considered: we take 70 sites on the left to mimic the atoms of the metallic electrode and the other 90 sites on the right for the organic molecules, respectively. Moreover, as a crucial consideration of this work, we note that the morphology of the interface is essential for charge injection. Specifically, as organic materials are normally soft and amorphous, there is a remarkable permeability of organic molecules into the metallic electrode. Therefore, a certain number of sites in the electrode close to the organic side will be regarded as an interfacial layer. It is worth noting that our approach can be safely applied to higher-dimensional systems, but at much greater computational cost than in the current work. As the molecular crystal normally forms a quasi-one-dimensional π/π stacking structure, the present model structure should be regarded as applicable.

The model Hamiltonian consists of three terms, as follows:

$$H = H_{\text{ele}} + H_{\text{lat}} + H_{\text{ext}}. \quad (1)$$

The first term in Eq. (1) is the electronic Hamiltonian, expressed as

$$H_{\text{ele}} = - \sum_n t_n (\hat{c}_{n+1}^\dagger \hat{c}_n + \text{h.c.}), \quad (2)$$

where \hat{c}_n^\dagger (\hat{c}_n) creates (annihilates) an electron at the n th site and $t_n = t_{0(1)} - \alpha_n(u_{n+1} - u_n)$ is the nearest-neighbor hopping integral in which the vibronic coupling is involved, namely, with α_n being the vibronic coupling strength and u_n being the displacement of the n th site. Herein, t_0 is the hopping constant in both the electrode and the organic material and t_1 is the coupling between them. Figure 1(b) displays the spatial distribution of α_n at each site of the metal-organic heterojunction. The vibronic coupling $\alpha_n = 0$ for metallic sites far away from interface, so that it is gapless. For the organic molecules, we take uniform vibronic couplings, namely $\alpha_n = \alpha$, so that the initial state of the organic molecules is dimerized due to the Peierls instability and the gap is determined by the value of α . In this situation, there naturally exists a barrier between the electrode and the organic material. In the interfacial layer, the vibronic coupling strength on the side of the metallic electrode is given by a half-Gaussian function, namely,

$$\alpha_n = \alpha \exp[-4(n - n_0)^2/W^2], \quad (3)$$

where n_0 is the last site of the metallic electrode and W is the width of the interfacial layer. Here, W is an essential parameter in our model to characterize the interface, which is defined as the width of the half-Gaussian function.

The second term in Eq. (1) represents the elastic potential and kinetic energy of the molecules:

$$H_{\text{lat}} = \frac{K}{2} \sum_n (u_{n+1} - u_n)^2 + \frac{M}{2} \sum_n \dot{u}_n^2, \quad (4)$$

where K is the elastic constant and M is the mass of the molecules.

The third term of Eq. (1) describes the contribution from the external field and has the following form:

$$H_{\text{ext}} = \sum_n U_n(t) \hat{c}_n^\dagger \hat{c}_n, \quad (5)$$

where $U_n(t)$ is the potential energy induced by the applied bias voltage and the electric field. In the metallic electrode, a bias voltage is applied and written as $U_n(t) = |e|V(t)$. In the organic molecules, an electric field $E_n(t)$ along the $-\hat{x}$ direction is thus generated and then the potential energy is determined by $U_n(t) = -|e|V_n(t)$. As another important input of our approach, we consider embedding the device modeling into the dynamic simulations. That is, considering the feedback of the distribution of the injected charges onto the electric field, $E_n(t)$ and $V_n(t)$ are given by Poisson's equation [45–47]:

$$E_n(t) = E_{n-1}(t) - \frac{|e|a_0\rho_n(t)}{\varepsilon_r\varepsilon_0V_{\text{rub}}}, \quad V_n(t) = V_{n-1}(t) - E_n(t)a_0, \quad (6)$$

where e is the elementary charge of an electron, ε_r is the relative dielectric constant, ε_0 is the permittivity of vacuum, a_0 is the lattice constant, V_{rub} is the occupying volume of a single molecule, and ρ_n is the injected charges at the n th site. In the practical simulations, in order to minimize the numerical errors, we turn on the external field smoothly by using a half-Gaussian function, that is, $V(t) = V_0 \exp[-(t - t_c)^2/t_w^2]$ for $0 < t < t_c$ and $V(t) = V_0$ for $t \geq t_c$, where t_c is a smooth turn-on period and t_w is the width. We set $t_c = 30$ fs and $t_w = 25$ fs, which are optimum values for numerical accuracy through our testing. The electric field $E_1(t)$ at the first organic molecule is also turned on smoothly in the same way and the initial value E_1 is determined by $V_0 = La_0E_1$, with L being the site number of the organic molecules.

The model parameters in this work are obtained from the earlier work by Troisi for investigating the charge transport of rubrene, namely, $t_0 = 1150$ cm⁻¹, $\alpha = 3980$ cm⁻¹/Å, $K = 48\,200$ amu/ps², $M = 532$ amu [17], $a_0 = 3.4$ Å, and $V_{\text{rub}} = 760$ Å³, according to our computations. For most organic materials, the dielectric constant normally ranges between 3 and 4 [48] and we set it to 4 in this work. For description of the metal-organic interface with a potential barrier, we set $t_1 = 0.8t_0$.

The motion of the sites can be described by the Newtonian equation. As we want to concurrently take the

thermionic emission into account, the temperature should also be involved as a parameter in our model. Hence, the Langevin equation is employed, as follows:

$$\begin{aligned} F_n(t) = M\ddot{u}_n = & -K[2u_n - u_{n+1} - u_{n-1}] \\ & + \alpha_n[\rho_{n,n+1} - \rho_{n-1,n} + \rho_{n+1,n} - \rho_{n,n-1}] \\ & - \gamma M\dot{u} + \xi_n, \end{aligned} \quad (7)$$

where $F_n(t)$ represents the force exerted on the n th site, the density matrix ρ is given by $\rho_{n,n'} = \sum_{\mu} \psi_{\mu,n}^*(t) f_{\mu} \psi_{\mu,n'}(t)$, in which f_{μ} (equal to 0, 1, or 2) is the time-independent distribution function determined by the initial occupation of electrons, γ is the friction coefficient, which is set to 0.01 ps^{-1} , and ξ_n is a Markovian Gaussian random force with standard deviation $(2\gamma M k_B T / \Delta t)^{1/2}$ to mimic the thermal effect. With these considerations, the lattice displacement $u_n(t_{j+1})$ and the velocity $\dot{u}_n(t_{j+1})$ are, respectively, given by

$$\begin{aligned} u_n(t_{j+1}) &= u_n(t_j) + \dot{u}_n(t_j) \Delta t, \\ \dot{u}_n(t_{j+1}) &= \dot{u}_n(t_j) + \frac{F_n(t_j)}{M} \Delta t. \end{aligned} \quad (8)$$

The time evolution of the electronic wave function is given by the time-dependent Schrödinger equation:

$$i\hbar \frac{\partial \psi_{\mu,n}(t)}{\partial t} = -t_n \psi_{\mu,n+1}(t) - t_{n-1} \psi_{\mu,n-1}(t), \quad (9)$$

where $\psi_{\mu,n}$ is the μ th eigenstate of the Hamiltonian (1) at the n th site. Herein, in order to numerically solve the electronic wave function, the integration time step Δt in the discretization procedure must be set to be sufficiently small, namely, below the order of magnitude of the bare phonon frequency $\omega_Q = \sqrt{4K/M}$. It is thus set to be 0.2 fs except for the trivial crossings. Therefore, the solution of the time-dependent Schrödinger equation is finally written as [49]

$$\psi_{\mu}(t_{j+1}) = \sum_{\nu} \langle \varphi_{\nu} | \psi_{\mu}(t_j) \rangle \exp[-i\varepsilon_{\nu} \Delta t / \hbar] \varphi_{\nu}, \quad (10)$$

where φ_{ν} and ε_{ν} are the instantaneous eigenfunctions and eigenvalues of the Hamiltonian, respectively.

The eigenfunctions of the Hamiltonian can be expressed with the original diabatic orbitals, $\varphi_{\nu} = \sum_n p_{n,\nu} |n\rangle$. The electronic wave function is described using a linear expansion of these eigenfunctions, $\psi = \sum_{\nu} c_{\nu} \varphi_{\nu}$. The time-dependent Schrödinger equation is then written as

$$\dot{c}_{\nu} = \frac{1}{i\hbar} c_{\nu} \varepsilon_{\nu} - \sum_{\mu \neq \nu} c_{\mu} \sum_n \dot{u}_n d_{\nu,\mu}^n, \quad (11)$$

where $d_{\nu,\mu}^n = \langle \varphi_{\nu} | d\varphi_{\mu} / du_n \rangle$ is the nonadiabatic coupling, which is obtained by the Hellmann-Feynman theorem, i.e.,

$$d_{\nu,\mu}^n = \frac{\alpha_n [p_{n,\nu} (p_{n-1,\mu} - p_{n+1,\mu}) + p_{n,\mu} (p_{n-1,\nu} - p_{n+1,\nu})]}{\varepsilon_{\mu} - \varepsilon_{\nu}}. \quad (12)$$

If the quantumness of the system is strong enough, the charge injection will be dominated by the quantum tunneling, which is highlighted by the fact that the nonadiabatic transitions among different PESs adhere to the electrode and organic molecules, respectively. In inorganic semiconductors, one can simply consider a scattering process through, for example, a triangle-shaped energy barrier to simulate this tunneling effect. In organic semiconductors, however, the electron is self-trapped and relatively localized such that it is not easy for the electrons to hop across the barriers due to their own kinetic energy and the electron-phonon interactions normally serve as the main driving force to induce the quantum tunneling. To this end, we have to adopt Tully's standard SH algorithm to take this tunneling effect into account in the simulations and the hopping probability from the active surface ν to another surface μ is given by [32]

$$g_{\nu,\mu} = \Delta t \times \frac{2 \text{Re}(c_{\nu} c_{\mu}^* \sum_n \dot{u}_n d_{\nu,\mu}^n)}{c_{\nu}^* c_{\nu}}. \quad (13)$$

If $g_{\nu,\mu} < 0$, it is reset to be zero. A uniform random number ζ is generated and then a surface hop takes place if $\sum_{X \neq \nu}^{\mu-1} g_{\nu,X} < \zeta \leq \sum_{X \neq \nu}^{\mu} g_{\nu,X}$. A velocity adjustment is then made to conserve the total energy if $\varepsilon_{\mu} - \varepsilon_{\nu} < (M/2) \sum_n \dot{u}_n^2$, i.e.,

$$\dot{u}'_n = \dot{u}_n + d_{\nu,\mu}^n \frac{A}{B} \left[\sqrt{1 + 2(\varepsilon_{\nu} - \varepsilon_{\mu}) \frac{B}{A^2}} - 1 \right], \quad (14)$$

where $A = \sum_n M \dot{u}_n d_{\nu,\mu}^n$ and $B = \sum_n M d_{\nu,\mu}^n d_{\nu,\mu}^n$. It is noted that the hop cannot occur if $\varepsilon_{\nu} < \varepsilon_{\mu} - A^2/2B$.

It is known that trivial crossings are very common in large systems involving many electronic states due to the rapid change with time of the nonadiabatic couplings [50,51]. Adaptive time intervals [33,51–53] and manual surface hops [51,54] have been proven to be valid in SH simulations to deal with the trivial crossings. Considering the computational cost and the size of our model system, we first adjust Δt to be 0.02 fs for the calculation of the explicit hopping probabilities and then make manual hops if Δt is not small enough. For simplicity, we only consider the electron residing on top of the Fermi surface, which stochastically hops from the active PES to another in a time step. To obtain smooth averaged curves of the time-dependent injected charges, 100 realizations for each simulation are performed.

III. RESULTS AND DISCUSSION

We first discuss the dynamical process of the injected charges in the organic molecules. By using the SH algorithm, we calculate the injected charge distribution $\rho_n(t)$ and the corresponding electric field distribution $E_n(t)$ in the organic molecules at different time points with interfacial width $W = 20a_0$, bias voltage $V_0 = 5$ V, and temperature $T = 300$ K. As shown in Fig. 2(a), driven by the applied bias voltage, charges initially residing in the metallic electrode are injected into the organic molecules by overcoming the interfacial barrier induced by the Peierls instability and then quickly spread onto the whole of the organic molecules. Afterward, enforced by the built-in electric field $E_n(t)$, the injected charges are redistributed and accumulated on the left-hand side of the organic molecules, near the metal-organic interface, after a relaxation time of approximately 80 fs. This is because we do not consider the other electrodes in the devices, such that there is no drain for the carriers; we are dealing with a single contact for the first step. From Fig. 2(b), one can find that $E_n(t)$ becomes larger as more charges are injected into the organic layer, which in turn further promotes the redistribution of the injected charges. It is known that the formation of stable localized polarons generally takes place in the charge-injection process in π -conjugated polymers such as polyacetylene [27,29,30,55]. However, it is also reported that the transport characteristics of molecular crystals, such as pentacene and rubrene, generally show high mobility and delocalized quantum carriers [56–59], which is quite different from the situation in the π -conjugated polymers. Benefitting from the utilization of the quantum dynamic approach combined with Poisson’s equation, the phenomenon of the transition from dispersive to localized features of the injected charges in organic

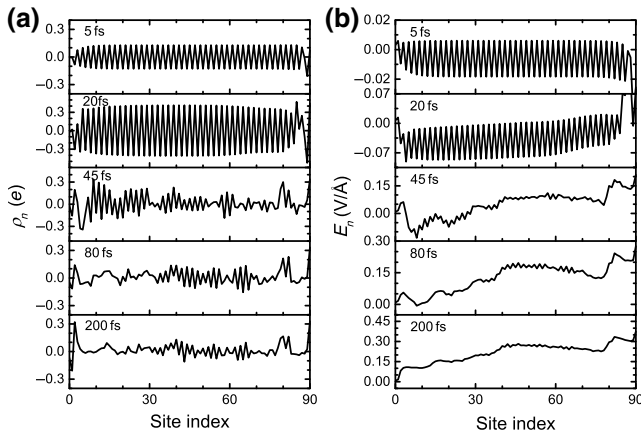


FIG. 2. (a) The injected charge distribution $\rho_n(t)$ and (b) the corresponding electric field distribution $E_n(t)$ in the organic molecules at different time points, with $W = 20a_0$, $V_0 = 5$ V, and $T = 300$ K.

molecular materials under the applied bias voltage can be simulated well.

In order to show the crucial role of quantum tunneling in charge injection, we give a comparison of the efficiency for charge injection at metal-organic interfaces by individually using the SH algorithm and the Ehrenfest dynamic approach. Figure 3 displays the time evolution of the injected charges Q at four typical temperatures, ranging from low to high. The other parameters are $W = 20a_0$ and $V_0 = 5$ V. One can observe that Q increases gradually with the evolution time and finally converges to different values at several hundreds of femtoseconds. The noticeable differences in the dynamic properties for these two methods should be emphasized. It can be found from Fig. 3(a) that Q calculated by the Ehrenfest dynamics is larger than that calculated by the SH algorithm at ultralow temperature, $T = 7.5$ K. However, as the temperature increases, Q calculated by the SH algorithm becomes close to that of the Ehrenfest dynamics at $T = 20$ K [see Fig. 3(b)] and

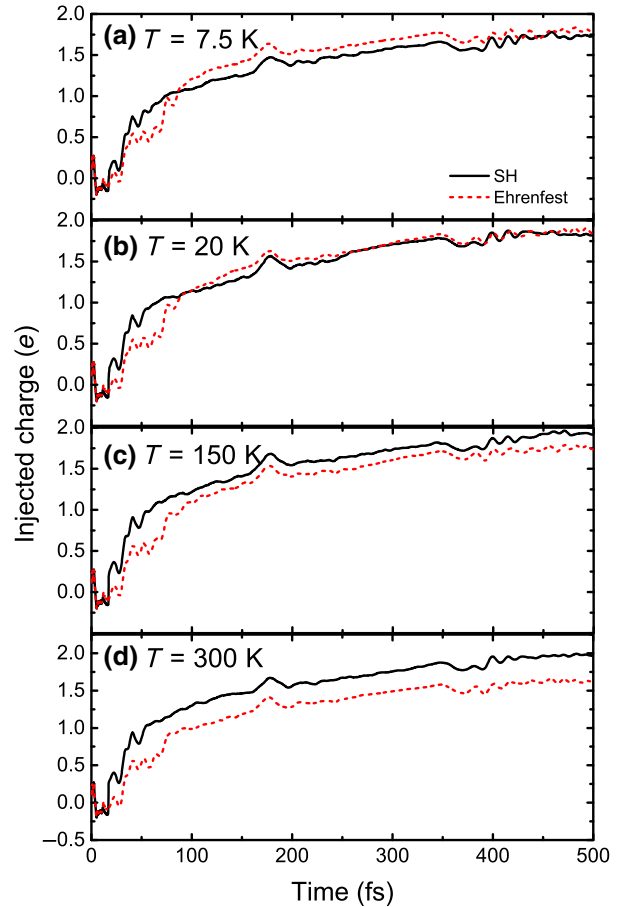


FIG. 3. The time evolution of the charge injected into the organic molecules for various temperatures $T =$ (a) 7.5 K, (b) 20 K, (c) 150 K, and (d) 300 K for the comparison between the SH algorithm and the Ehrenfest dynamics. The other parameters are $W = 20a_0$ and $V_0 = 5$ V.

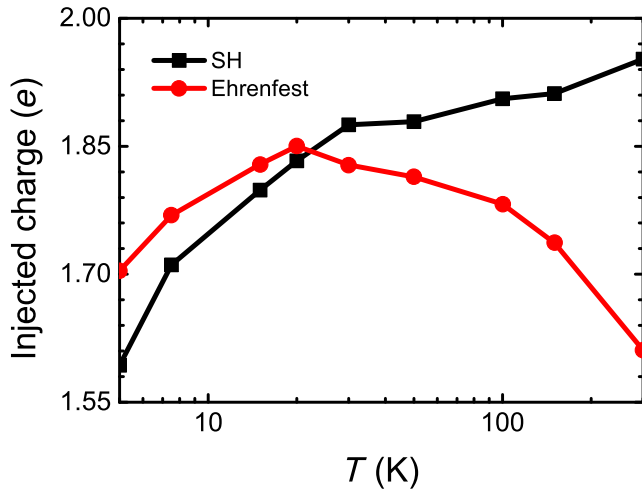


FIG. 4. The injected charge versus the temperature for the comparison between the SH algorithm and the Ehrenfest dynamics with $W = 20a_0$ and $V_0 = 5$ V.

then starts to be larger at $T = 150$ K and $T = 300$ K [see Figs. 3(c) and 3(d), respectively] due to the quantum tunneling represented by the nonadiabatic transition between PESs adhering to the electrode and organic molecules.

To further manifest the advantages of the SH algorithm for simulating charge injection, we calculate the mean value of the injected charges Q over the smooth time range between 400 fs and 500 fs for more typical temperatures. Figure 4 shows the temperature dependence of Q obtained by the SH algorithm and the Ehrenfest dynamics with $W = 20a_0$ and $V_0 = 5$ V. The curves can be analyzed in two different temperature regimes. One is from 5 K to 30 K, in which Q obtained by the Ehrenfest dynamics is slightly larger than that from the SH algorithm, and the other is from 30 K to 300 K, in which the Q obtained by the SH algorithm is significantly larger. More importantly, the temperature dependence of the injected charges calculated from the Ehrenfest dynamics shows a counterintuitive result that the charge-injection efficiency decreases with increasing temperature, so we can conclude that the Ehrenfest dynamics break down at room temperature. The processes of both the SH algorithm and the Ehrenfest dynamics are schematically illustrated in Fig. 5. Due to the Peierls instability and the resulting energy gap, as stated above, the PES of the organic molecules is higher than that of the interface in the metallic electrode. At low temperature, the nonadiabatic transitions are largely suppressed, so the pathway $P_{\text{SH,LT}}$ is predominant. In this situation, since the mean-field treatment of PESs in the Ehrenfest dynamics gives rise to a higher pathway $P_{\text{Ehrenfest}}$ than that of the SH algorithm, the charge injection from the Ehrenfest dynamics exhibits a slightly higher efficiency. At room temperature, on the other hand, nonadiabatic transitions obviously win out, so that the pathway

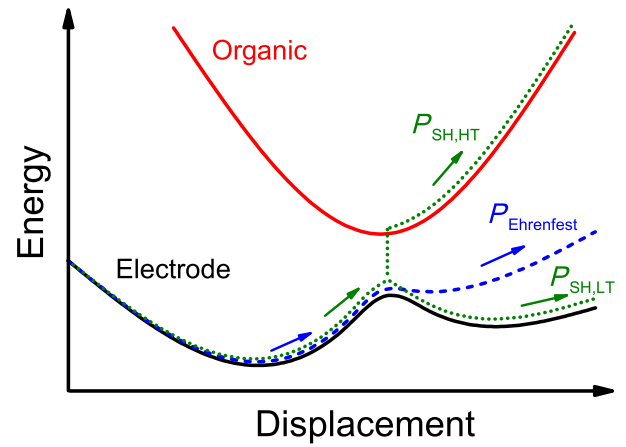


FIG. 5. A schematic representation of the PESs of the metal-organic heterojunction with respect to the displacement of the sites. The PES of the organic molecules (red solid) is higher than that of the interface in the metallic electrode (black solid) due to the initial energy gap in the organic semiconductor. $P_{\text{Ehrenfest}}$ (blue dashed) denotes the pathway of the Ehrenfest dynamics for charge injection. Two pathways of the SH algorithm for charge injection can be recognized: one is $P_{\text{SH,LT}}$, the main pathway at low temperature (lower green dotted) and the other is $P_{\text{SH,HT}}$, which is mainly for high temperature (upper green dotted).

$P_{\text{SH,HT}}$ turns out to be the main channel for charge injection. From Fig. 4, it is also found that the line shape deviates from that of the Richardson formula, namely, approximately $T^2 \exp(-\phi/k_B T)$, where ϕ is the injection barrier. Our result exhibits larger injection efficiency than that derived from the Richardson formula within 30–300 K, which is explicitly the consequence of involving quantum effects. We note that, following the traditional line of research on metal-semiconductor contacts, herein we merely consider injection from a single electrode and there is no drain for the injected charges. In a realistic experiment, the temperature-dependent mobility influenced by the dynamic disorder would also greatly affect the injection efficiency, making the practical measurement results change dramatically over an extensive temperature regime. This device effect will be taken into account in our future work for more complete and comprehensive device modeling.

For the sake of device modeling, our dynamic approach has to work with the influence of the bias voltage V_0 , applied at the metallic electrode, on the charge-injection efficiency. To this end, three different values of W are chosen for the calculation of the total injected charges at $T = 300$ K, which is displayed in Fig. 6. The figure shows a monotonic increase of Q with the increase of V_0 for three values of W . When a larger V_0 is applied at the metallic electrode, the initial electric field in the organic layer becomes larger, which has a stronger promoting effect for charge injection. Surprisingly, when the

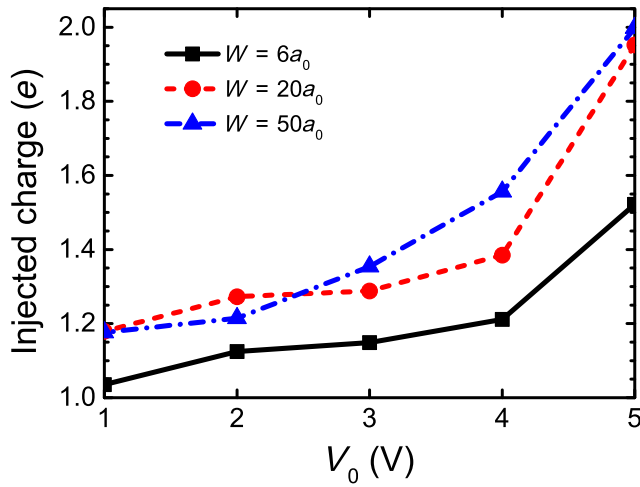


FIG. 6. The injected charge versus the applied bias voltage V_0 by using the SH algorithm for various interfacial widths W with $T = 300$ K.

value of V_0 is low, at 1 V, which is about half of the band gap of rubrene (approximately 2.2 eV), the charges can still be injected into the organic molecules efficiently. In spite of the combined electric field simulation in our model, this result shows the low-threshold injection characteristics of these molecular crystals such as rubrene, which are quite in agreement with the experimental results [40–44]. Moreover, from Fig. 6, one can also find that Q becomes larger when the larger W is applied in the high- V_0 range, while the trend is not obvious when V_0 is lower than 3 V, implying that the efficiency of charge injection at metal-organic interfaces is closely related to the width of the interfacial layer, which should be further investigated.

As is well known, interfaces are essential for organic semiconductors in both fundamental researches and applications. In our previous work, we have discussed an optimum width of the donor-acceptor (D/A) interface for dissociation of the charge-transfer (CT) state [49]. In the practical fabrication of devices, the insertion of a buffer layer between the metallic electrode and the organic layer can effectively facilitate the injection of charge [60–63] and Hou’s group has obtained an optimal buffer layer width of several nanometers, based on both model calculations and experimental investigations [60]. Here, with our dynamic approach, we can also determine an optimum width of the metal-organic interface for charge injection. Figure 7 displays the injected charges Q for various interfacial widths at certain values of V_0 with $T = 300$ K. For the cases of $V_0 = 3$ V and $V_0 = 4$ V, with the increase of the interfacial width, Q increases dramatically for $W < 30a_0$, followed by a remarkable decrease. Differently, for the case of $V_0 = 5$ V, Q first dramatically increases and then undergoes a slight increase, except for the case $W = 40a_0$.

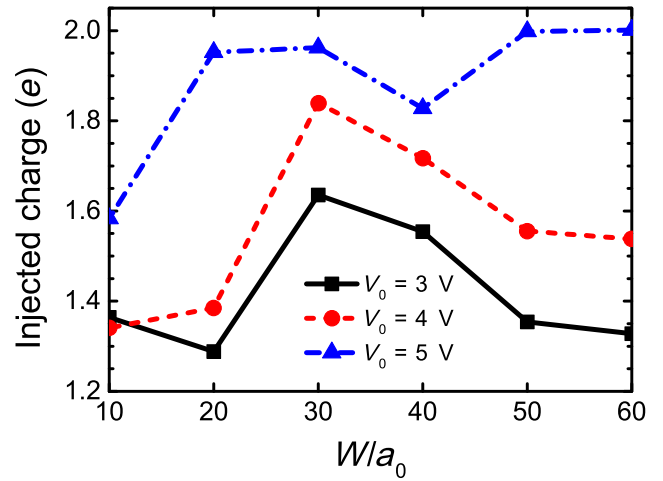


FIG. 7. The injected charge versus the interfacial width W by using the SH algorithm for various bias voltages V_0 with $T = 300$ K.

As a consequence here, the optimum value of the interfacial width for charge injection is determined to be $30a_0$ (approximately 10 nm) in our case, which is consistent with Hou’s results [60].

Finally, we would like to discuss the quantumness of the charge-injection process at metal-organic interfaces in more detail. As stated above, the classical thermionic emission theory cannot be directly applied to organic semiconductors; lots of quantum effects have been discussed in these systems, especially taking photoemission into consideration [21,22,64]. To this end, we calculate the von Neumann entropy of the injected charges, which is defined as [65,66]

$$S_L = -\text{Tr}(\rho_L \ln \rho_L), \quad (15)$$

where ρ_L is the reduced density matrix of the charges in the organic molecules. Figure 8 exhibits the time evolution of the von Neumann entropy S_L of the system during the charge-injection process, with $W = 20a_0$, $V_0 = 5$ V, and $T = 300$ K. It is found that S_L increases gradually with the evolution time and finally saturates to a constant. We note that the total increase of the entropy is roughly 3%, which is not significant compared with our expectation that following the injection of more charges, the entropy will largely increase, so that the quantumness will quickly be lost. In our previous work, we have also presented a coherent scenario for dissociation of the CT state at the D/A interfaces in organic photovoltaics [49]. Combining these two studies, our findings may enlighten the understanding of the quantumness of charge dynamics in organic semiconductors, which may facilitate the establishment of a systematic device-modeling method specifically for this system.

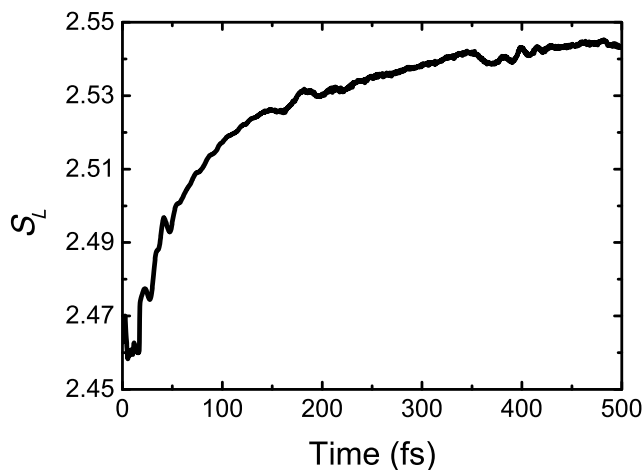


FIG. 8. The time evolution of the von Neumann entropy S_L of the injected charges with $W = 20a_0$, $V_0 = 5$ V, and $T = 300$ K.

IV. CONCLUSION AND OUTLOOK

In summary, we develop a unified dynamic approach based upon the SH algorithm combined with Poisson's equation to investigate the charge-injection process at the metal-organic interface. We find that the charges can be dynamically injected into the organic materials and then quickly spread onto the molecules in a dispersive fashion, followed by an accumulation induced by the built-in electric field. The injected charges obtained by the SH algorithm are compared with those resulting from the Ehrenfest dynamics, and the former method works well for simulating efficient charge injection at room temperature, while the latter method is merely valid at ultralow temperature. The influence of the bias voltage applied at the metallic electrode on the charge-injection efficiency is discussed and the injected charges undergo a significant increase with an increasing applied bias voltage. With the assistance of the quantum effect, the charges can be injected into the organic molecules efficiently even if the bias voltage is small compared with the band gap of the organic material, which can be utilized to explain the low-threshold feature. The width of approximately 10 nm is regarded as the optimum value of the interfacial layer for charge injection at metal-organic interfaces. In addition, the von Neumann entropy provides a further insight into the quantumness of the charge-injection dynamics.

In inorganic semiconductors, thermal equilibrium is basically valid in an approximate manner, since the thermal motions of the atoms are almost completely disordered. In contrast, the molecular vibrations in organic materials are always concentrated into some specific modes, so that the quantum coherence of the electrons could be well protected in order to keep the quantumness alive. In organic photovoltaic devices, coherent exciton dynamics have been demonstrated in many experiments

and widely discussed [67–70]. As the majority charge carriers in organic semiconductors stem from injection at the interfaces rather than doping, the normal thermionic emission theory is not sufficient for us to understand the conductivity in these devices. A dynamic scenario serves as an alternative perspective. It is worth noting that, in earlier research, *ab initio* nonadiabatic molecular dynamics have been developed by Prezhdo's group to deal with the dynamic processes of charge injection [71,72]—however, only considering a second-order differencing scheme rather than surface hopping. With the present unified dynamic approach in hand, we can in the future establish a systematic device-modeling method to mimic the device performance and yield the material parameters obtained from quantum-chemistry computations. We believe that this first-principles framework could help us to simulate organic semiconducting devices in a more appropriate and efficient way.

ACKNOWLEDGMENTS

We gratefully acknowledge support from the National Natural Science Foundation of China (Grants No. 91833305 and No. 11974118), the Key Research and Development Project of Guangdong Province (Grant No. 2020B0303300001) and the Fundamental Research Funds for the Central Universities (Grant No. 2019ZD51).

- [1] F. Huang, H. Wu, and Y. Cao, Water/alcohol soluble conjugated polymers as highly efficient electron transporting/injection layer in optoelectronic devices, *Chem. Soc. Rev.* **39**, 2500 (2010).
- [2] B. R. Lee, J.-w. Kim, D. Kang, D. W. Lee, S.-J. Ko, H. J. Lee, C.-L. Lee, J. Y. Kim, H. S. Shin, and M. H. Song, Highly efficient polymer light-emitting diodes using graphene oxide as a hole transport layer, *ACS Nano* **6**, 2984 (2012).
- [3] Q. Wang, Y. Zhou, H. Zheng, J. Shi, C. Li, C. Q. Su, L. Wang, C. Luo, D. Hu, J. Pei, J. Wang, J. Peng, and Y. Cao, Modifying organic/metal interface via solvent treatment to improve electron injection in organic light emitting diodes, *Org. Electron.* **12**, 1858 (2011).
- [4] Z. Zhong, Z. Hu, Z. Jiang, J. Wang, Y. Chen, C. Song, S. Han, F. Huang, J. Peng, J. Wang, and Y. Cao, Hole-trapping effect of the aliphatic-amine based electron injection materials in the operation of OLEDs to facilitate the electron injection, *Adv. Electron. Mater.* **1**, 1400014 (2015).
- [5] Z. Hu, Z. Zhong, K. Zhang, Z. Hu, C. Song, F. Huang, J. Peng, J. Wang, and Y. Cao, Dipole formation at organic/metal interfaces with pre-deposited and post-deposited metal, *NPG Asia Mater.* **9**, e379 (2017).
- [6] G. A. H. Wetzelaer and P. W. M. Blom, Ohmic current in organic metal-insulator-metal diodes revisited, *Phys. Rev. B* **89**, 241201(R) (2014).
- [7] C. G. Tang, M. C. Y. Ang, K. K. Choo, V. Keerthi, J. K. Tan, M. N. Syafiqah, T. Kugler, J. H. Burroughes, R. Q. Png, L.

- L. Chua, and P. K. Ho, Doped polymer semiconductors with ultrahigh and ultralow work functions for ohmic contacts, *Nature* **539**, 536 (2016).
- [8] N. B. Kotadiya, H. Lu, A. Mondal, Y. Ie, D. Andrienko, P. W. M. Blom, and G. A. H. Wetzelaer, Universal strategy for Ohmic hole injection into organic semiconductors with high ionization energies, *Nat. Mater.* **17**, 329 (2018).
- [9] G. Xu, N. Gao, C. Lu, W. Wang, Z. Ji, C. Bi, Z. Han, N. Lu, G. Yang, Y. Li, Q. Liu, L. Li, and M. Liu, Bulk-like electrical properties induced by contact-limited charge transport in organic diodes: Revised space charge limited current, *Adv. Electron. Mater.* **4**, 1700493 (2018).
- [10] S. M. Sze, *Physics of Semiconductor Devices* (Wiley, New York, 1981).
- [11] N. Koch and A. Vollmer, Electrode-molecular semiconductor contacts: Work-function-dependent hole injection barriers versus Fermi-level pinning, *Appl. Phys. Lett.* **89**, 162107 (2006).
- [12] W. Osikowicz, M. P. de Jong, S. Braun, C. Tengstedt, M. Fahlman, and W. R. Salaneck, Energetics at Au top and bottom contacts on conjugated polymers, *Appl. Phys. Lett.* **88**, 193504 (2006).
- [13] C. Tengstedt, W. Osikowicz, W. R. Salaneck, I. D. Parker, C.-H. Hsu, and M. Fahlman, Fermi-level pinning at conjugated polymer interfaces, *Appl. Phys. Lett.* **88**, 053502 (2006).
- [14] A. Crispin, X. Crispin, M. Fahlman, M. Berggren, and W. R. Salaneck, Transition between energy level alignment regimes at a low band gap polymer-electrode interfaces, *Appl. Phys. Lett.* **89**, 213503 (2006).
- [15] K. Stokbro and S. Smidstrup, Electron transport across a metal-organic interface: Simulations using nonequilibrium Green's function and density functional theory, *Phys. Rev. B* **88**, 075317 (2013).
- [16] A. Troisi and G. Orlandi, Charge-transport regime of crystalline organic semiconductors: Diffusion limited by thermal off-diagonal electronic disorder, *Phys. Rev. Lett.* **96**, 086601 (2006).
- [17] A. Troisi, Prediction of the absolute charge mobility of molecular semiconductors: The case of rubrene, *Adv. Mater.* **19**, 2000 (2007).
- [18] L. Wang, D. Beljonne, L. Chen, and Q. Shi, Mixed quantum-classical simulations of charge transport in organic materials: Numerical benchmark of the Schrieffer-Heeger model, *J. Chem. Phys.* **134**, 244116 (2011).
- [19] L. Wang, A. V. Akimov, L. Chen, and O. V. Prezhdo, Quantized Hamiltonian dynamics captures the low-temperature regime of charge transport in molecular crystals, *J. Chem. Phys.* **139**, 174109 (2013).
- [20] L. Wang and D. Beljonne, Charge transport in organic semiconductors: Assessment of the mean field theory in the hopping regime, *J. Chem. Phys.* **139**, 064316 (2013).
- [21] M. Barbatti, Nonadiabatic dynamics with trajectory surface hopping method, *WIREs Comput. Mol. Sci.* **1**, 620 (2011).
- [22] J. E. Subotnik, A. Jain, B. Landry, A. Petit, W. Ouyang, and N. Bellonzi, Understanding the surface hopping view of electronic transitions and decoherence, *Annu. Rev. Phys. Chem.* **67**, 387 (2016).
- [23] J. C. Tully, Perspective: Nonadiabatic dynamics theory, *J. Chem. Phys.* **137**, 22A301 (2012).
- [24] L. Wang, O. V. Prezhdo, and D. Beljonne, Mixed quantum-classical dynamics for charge transport in organics, *Phys. Chem. Chem. Phys.* **17**, 12395 (2015).
- [25] L. Wang, A. Akimov, and O. V. Prezhdo, Recent progress in surface hopping: 2011–2015, *J. Phys. Chem. Lett.* **7**, 2100 (2016).
- [26] L. Wang, J. Qiu, X. Bai, and J. Xu, Surface hopping methods for nonadiabatic dynamics in extended systems, *WIREs Comput. Mol. Sci.* **10**, e1435 (2019).
- [27] C. Q. Wu, Y. Qiu, Z. An, and K. Nasu, Dynamical study on polaron formation in a metal/polymer/metal structure, *Phys. Rev. B* **68**, 125416 (2003).
- [28] Y. H. Yan, Z. An, C. Q. Wu, and K. Nasu, Formation dynamics of bipolaron in a metal/polymer/metal structure, *Eur. Phys. J. B* **48**, 501 (2005).
- [29] A. A. Johansson and S. Stafström, Nonadiabatic simulations of polaron dynamics, *Phys. Rev. B* **69**, 235205 (2004).
- [30] J.-y. Fu, J.-f. Ren, X.-j. Liu, D.-s. Liu, and S.-j. Xie, Dynamics of charge injection into an open conjugated polymer: A nonadiabatic approach, *Phys. Rev. B* **73**, 195401 (2006).
- [31] L. A. Ribeiro Junior and W. F. da Cunha, Nonadiabatic dynamics of injected holes in conjugated polymers, *Phys. Chem. Chem. Phys.* **19**, 10000 (2017).
- [32] J. C. Tully, Molecular dynamics with electronic transitions, *J. Chem. Phys.* **93**, 1061 (1990).
- [33] L. Wang and D. Beljonne, Flexible surface hopping approach to model the crossover from hopping to band-like transport in organic crystals, *J. Phys. Chem. Lett.* **4**, 1888 (2013).
- [34] L. Wang and O. V. Prezhdo, A simple solution to the trivial crossing problem in surface hopping, *J. Phys. Chem. Lett.* **5**, 713 (2014).
- [35] L. Wang, D. Trivedi, and O. V. Prezhdo, Global flux surface hopping approach for mixed quantum-classical dynamics, *J. Chem. Theory Comput.* **10**, 3598 (2014).
- [36] A. E. Sifain, L. Wang, and O. V. Prezhdo, Mixed quantum-classical equilibrium in global flux surface hopping, *J. Chem. Phys.* **142**, 224102 (2015).
- [37] J. Qiu, X. Bai, and L. Wang, Crossing classified and corrected fewest switches surface hopping, *J. Phys. Chem. Lett.* **9**, 4319 (2018).
- [38] J. Qiu, X. Bai, and L. Wang, Subspace surface hopping with size-independent dynamics, *J. Phys. Chem. Lett.* **10**, 637 (2019).
- [39] X. Bai, J. Qiu, and L. Wang, An efficient solution to the decoherence enhanced trivial crossing problem in surface hopping, *J. Chem. Phys.* **148**, 104106 (2018).
- [40] A. K. Pandey and J.-M. Nunzi, Upconversion injection in rubrene/perylene diimide heterostructure electroluminescent diodes, *Appl. Phys. Lett.* **90**, 263508 (2007).
- [41] A. K. Pandey and J. M. Nunzi, Rubrene/fullerene heterostructures with a half-gap electroluminescence threshold and large photovoltage, *Adv. Mater.* **19**, 3613 (2007).
- [42] C. Xiang, C. Peng, Y. Chen, and F. So, Origin of sub-bandgap electroluminescence in organic light-emitting diodes, *Small* **11**, 5439 (2015).
- [43] Q. Chen, W. Jia, L. Chen, D. Yuan, Y. Zou, and Z. Xiong, Determining the origin of half-bandgap-voltage electroluminescence in bifunctional rubrene/C₆₀ devices, *Sci. Rep.* **6**, 25331 (2016).

- [44] S.-J. He and Z.-H. Lu, Ultralow-voltage Auger-electron-stimulated organic light-emitting diodes, *J. Photon. Energy* **6**, 036001 (2016).
- [45] C. Pflumm, C. Gartner, and U. Lemmer, A numerical scheme to model current and voltage excitation of organic light-emitting diodes, *IEEE J. Quantum Electron.* **44**, 790 (2008).
- [46] N. S. Christ, S. W. Kettlitz, S. Valouch, S. Züfle, C. Gärtner, M. Punke, and U. Lemmer, Nanosecond response of organic solar cells and photodetectors, *J. Appl. Phys.* **105**, 104513 (2009).
- [47] D. Li, L. Song, Y. Chen, and W. Huang, Modeling thin film solar cells: From organic to perovskite, *Adv. Sci.* **7**, 1901397 (2020).
- [48] V. I. Arkhipov and H. Bässler, Exciton dissociation and charge photogeneration in pristine and doped conjugated polymers, *Phys. Status Solidi A* **201**, 1152 (2004).
- [49] J. Huang, Y. Mo, and Y. Yao, Charge-transfer state dynamics in all-polymer solar cells: Formation, dissociation and decoherence, *Phys. Chem. Chem. Phys.* **21**, 2755 (2019).
- [50] G. Granucci, M. Persico, and A. Toniolo, Direct semi-classical simulation of photochemical processes with semiempirical wave functions, *J. Chem. Phys.* **114**, 10608 (2001).
- [51] S. Fernandez-Alberti, A. E. Roitberg, T. Nelson, and S. Tretiak, Identification of unavoided crossings in nonadiabatic photoexcited dynamics involving multiple electronic states in polyatomic conjugated molecules, *J. Chem. Phys.* **137**, 014512 (2012).
- [52] A. M. Virshup, B. G. Levine, and T. J. Martinez, Steric and electrostatic effects on photoisomerization dynamics using QM/MM *ab initio* multiple spawning, *Theor. Chem. Acc.* **133**, 1506 (2014).
- [53] L. Spörkel and W. Thiel, Adaptive time steps in trajectory surface hopping simulations, *J. Chem. Phys.* **144**, 194108 (2016).
- [54] E. Fabiano, T. W. Keal, and W. Thiel, Implementation of surface hopping molecular dynamics using semiempirical methods, *Chem. Phys.* **349**, 334 (2008).
- [55] S. V. Rakhmanova and E. M. Conwell, Polaron dissociation in conducting polymers by high electric fields, *Appl. Phys. Lett.* **75**, 1518 (1999).
- [56] V. Podzorov, E. Menard, J. A. Rogers, and M. E. Gershenson, Hall Effect in the Accumulation Layers on the Surface of Organic Semiconductors, *Phys. Rev. Lett.* **95**, 226601 (2005).
- [57] O. Ostroverkhova, D. G. Cooke, F. A. Hegmann, J. E. Anthony, V. Podzorov, M. E. Gershenson, O. D. Jurchescu, and T. T. M. Palstra, Ultrafast carrier dynamics in pentacene: Functionalized pentacene, tetracene, and rubrene single crystals, *Appl. Phys. Lett.* **88**, 162101 (2006).
- [58] T. Minari, T. Nemoto, and S. Isoda, Temperature and electric-field dependence of the mobility of a single-grain pentacene field-effect transistor, *J. Appl. Phys.* **99**, 034506 (2006).
- [59] M. E. Gershenson, V. Podzorov, and A. F. Morpurgo, Colloquium: Electronic transport in single-crystal organic transistors, *Rev. Mod. Phys.* **78**, 973 (2006).
- [60] S. T. Zhang, X. M. Ding, J. M. Zhao, H. Z. Shi, J. He, Z. H. Xiong, H. J. Ding, E. G. Obbard, Y. Q. Zhan, W. Huang, and X. Y. Hou, Buffer-layer-induced barrier reduction: Role of tunneling in organic light-emitting devices, *Appl. Phys. Lett.* **84**, 425 (2004).
- [61] T.-F. Guo, F.-S. Yang, Z.-J. Tsai, T.-C. Wen, S.-N. Hsieh, Y.-S. Fu, and C.-T. Chung, Organic oxide/Al composite cathode in efficient polymer light-emitting diodes, *Appl. Phys. Lett.* **88**, 113501 (2006).
- [62] T.-F. Guo, F.-S. Yang, Z.-J. Tsai, T.-C. Wen, C.-I. Wu, and C.-T. Chung, Organic oxide/Al composite cathode in small molecular organic light-emitting diodes, *Appl. Phys. Lett.* **89**, 053507 (2006).
- [63] T.-H. Lee, J.-C.-A. Huang, G. L. v. Pakhomov, T.-F. Guo, T.-C. Wen, Y.-S. Huang, C.-C. Tsou, C.-T. Chung, Y.-C. Lin, and Y.-J. Hsu, Organic-oxide cathode buffer layer in fabricating high-performance polymer light-emitting diodes, *Adv. Funct. Mater.* **18**, 3036 (2008).
- [64] T. Nelson, S. Fernandez-Alberti, A. E. Roitberg, and S. Tretiak, Nonadiabatic excited-state molecular dynamics: Modeling photophysics in organic conjugated materials, *Acc. Chem. Res.* **47**, 1155 (2014).
- [65] A. M. Läuchli and C. Kollath, Spreading of correlations and entanglement after a quench in the one-dimensional Bose-Hubbard model, *J. Stat. Mech.: Theor. Exp.* P05018 (2008).
- [66] L. Amico, R. Fazio, A. Osterloh, and V. Vedral, Entanglement in many-body systems, *Rev. Mod. Phys.* **80**, 517 (2008).
- [67] S. M. Falke, C. A. Rozzi, D. Brida, M. Maiuri, M. Amato, E. Sommer, A. De Sio, A. Rubio, G. Cerullo, E. Molinari, and C. Lienau, Coherent ultrafast charge transfer in an organic photovoltaic blend, *Science* **344**, 1001 (2014).
- [68] Y. Song, S. N. Clifton, R. D. Pensack, T. W. Kee, and G. D. Scholes, Vibrational coherence probes the mechanism of ultrafast electron transfer in polymer-fullerene blends, *Nat. Commun.* **5**, 4933 (2014).
- [69] Y. Song, C. Hellmann, N. Stingelin, and G. D. Scholes, The separation of vibrational coherence from ground- and excited-electronic states in P3HT film, *J. Chem. Phys.* **142**, 212410 (2015).
- [70] A. De Sio, F. Troiani, M. Maiuri, J. Rehault, E. Sommer, J. Lim, S. F. Huelga, M. B. Plenio, C. A. Rozzi, G. Cerullo, E. Molinari, and C. Lienau, Tracking the coherent generation of polaron pairs in conjugated polymers, *Nat. Commun.* **7**, 13742 (2016).
- [71] W. Stier and O. V. Prezhdo, Non-adiabatic molecular dynamics simulation of ultrafast solar cell electron transfer, *J. Mol. Struct. (THEOCHEM)* **630**, 33 (2003).
- [72] W. R. Duncan, W. M. Stier, and O. V. Prezhdo, *Ab initio* nonadiabatic molecular dynamics of the ultrafast electron injection across the Alizarin-TiO₂ interface, *J. Am. Chem. Soc.* **127**, 7941 (2005).